NASA TECHNICAL NOTE

NASA TN D-8374

ESTIMATES OF OPTIMAL OPERATING CONDITIONS FOR HYDROGEN-OXYGEN CESIUM-SEEDED MAGNETOHYDRODYNAMIC POWER GENERATOR

J. Marlin Smith and Lester D. Nichols

Lewis Research Center
Cleveland, Ohio 44135

NATIONAL AERONAUTICS AND SPACE ADMINISTRATION • WASHINGTON, D. C. • FEBRUARY 1977

1. Report No. NASA TN D-8374	2. Government Accession No.	3. Recipient's Catalog No.
4. Title and Subtitle ESTIMATES OF OPTIMAL OPERATING CONDITIONS FOR HYDROGEN-OXYGEN CESIUM-SEEDED MAGNETO-HYDRODYNAMIC POWER GENERATOR		5. Report Date February 1977 6. Performing Organization Code
7. Author(s) J. Marlin Smith and Lester D. Nichols		8. Performing Organization Report No. E-8828 10. Work Unit No. 506-25
9. Performing Organization Name and Address Lewis Research Center National Aeronautics and Space Administration Cleveland, Ohio 44135		11. Contract or Grant No. 13. Type of Report and Period Covered Technical Note
12. Sponsoring Agency Name and Address National Aeronautics and Space Administration Washington, D.C. 20546		14. Sponsoring Agency Code

15. Supplementary Notes

16. Abstract

In this study the value of percent seed, oxygen to fuel ratio, combustion pressure, Mach number, and magnetic field strength which maximize either the electrical conductivity or power density at the entrance of an MHD power generator were obtained. The working fluid is the combustion products of H_2 and O_2 seeded with CsOH. Two forms of the power density are investigated. The first is that of the ideal theoretical segmented Faraday generator. The second is an empirical form found from correlating the data of many experimenters working with generators of different sizes, electrode configurations, and working fluids. The conductivity and power densities optimize at a seed fraction of 3.5 mole percent and an oxygen to hydrogen weight ratio of 7.5. The optimum values of combustion pressure and Mach number depend on the operating magnetic field strength.

17. Key Words (Suggested by Author(s)) Magnetohydrodynamics Plasma physics	18. Distribution Statement Unclassified - unlimited STAR Category 75		
19. Security Classif. (of this report) Unclassified	20. Security Classif. (of this page) Unclassified	21. No. of Pages 36	22. Price* $4.00

* For sale by the National Technical Information Service, Springfield, Virginia 22161

ESTIMATES OF OPTIMAL OPERATING CONDITIONS FOR HYDROGEN-OXYGEN CESIUM-SEEDED MAGNETOHYDRODYNAMIC POWER GENERATOR

by J. Marlin Smith and Lester D. Nichols

Lewis Research Center

SUMMARY

In this study the value of percent seed, oxygen to hydrogen ratio, combustion pressure, Mach number, and magnetic field strength, which maximize either the electrical conductivity or power density at the entrance of an MHD power generator were obtained. The working fluid is the combustion products of hydrogen and oxygen seeded with cesium hydroxide (CsOH). Two forms of the power density are investigated: The first is that of the ideal theoretical segmented Faraday generator. The second is of an empirical form found from correlating the data of many experimenters working with generators of different sizes, electrode configurations, and working fluids.

The conductivity and power densities optimize at a seed fraction and an oxygen to fuel ratio in the neighborhood of 3.5 mole percent and 7.5, respectively. The optimum values of combustion pressure and Mach number depend on the operating magnetic field strength.

INTRODUCTION

In the practical design of a magnetohydrodynamic power generator for either mobile or base power applications, one parameter is of particular importance - size. The magnet size dominates the weight for mobile applications and the cost for base power applications. Therefore, it is desirable to operate the device with controllable conditions adjusted so as to obtain the maximum power density (smallest size for a specified power output).

In this study we considered a gaseous hydrogen and oxygen combustion working fluid seeded with cesium hydroxide (CsOH) dissolved in water. Hydrogen is desirable for lightweight mobile systems and was therefore chosen as a fuel because it has the highest

energy content per unit mass. Recent discussions of a hydrogen economy (ref. 1) indicate that it may also be a candidate for large base power systems.

The controllable parameters that are considered are the percent seed, oxygen to hydrogen ratio, combustion pressure, Mach number, and magnetic field strength. The operating values of these parameters that maximize either the electric conductivity or the power density at the entrance to the generator are presented.

Two forms of the power density are considered. The first is that of the ideal theoretical segmented Faraday generator. However, inasmuch as the presently measured power density of MHD generators is considerably below this ideal value, particularly in the region of large Hall parameters, an empirically derived formula was also considered. This empirical formula was found by correlating the data of many experimenters working with different generator sizes, electrode configurations, and working fluids. This correlation indicated that the broad base of data could be fitted by the ideal power density times a correction factor which depends solely on the Hall parameter.

A previous optimization study was reported in reference 2, where power density at the entrance was optimized as the first step in optimizing the entire MHD channel. In that case, however, an idealized hydrocarbon fuel burned in air was considered, the combustion gases were seeded with potassium sulphate, and only stoichiometric combustion was considered.

SYMBOLS

A conducting cross sectional area

B magnetic field strength

E electric field

e unit electric charge

h distance between Faraday electrodes

I electric current

j electric current density

K load parameter

k Boltzman constant

l distance between Hall electrodes

M Mach number

m mass

n number density

O/F oxygen to hydrogen weight ratio, eq. (16)

P power density

p gas pressure

$\langle Q_{ei} \rangle$ momentum transfer cross section between electron and i^{th} species

R electrical resistance

T gas temperature

T_i temperature corresponding to ionization potential

u gas flow velocity

V voltage

β Hall parameter

ν total electron collision frequency for momentum transfer

ν_{ei} momentum transfer collision frequency between electron and i^{th} species

σ electrical conductivity

φ tan α, where α is defined on fig. 2

Subscripts:

crit critical

D digital conducting wall

e electron

eff effective

F Faraday (used in appendix)

H Hall (used in appendix)

i i^{th} species

id ideal

m maximum

n neutral particle

S shorting

s seed particle

x Hall

y Faraday

ANALYSIS

Performance Parameters to be Optimized

The purpose of this study is to establish the operating conditions for a hydrogen-oxygen, cesium seeded MHD generator based on the optimization of the generator inlet conditions. The optimization of three quantities is considered. The first quantity is the electrical conductivity since its optimization will give the maximum current density for a given electric field.

The second quantity is the ideal power density. For the Faraday type of generator (ref. 3) that will be considered here, the ideal power density (obtained when the load resistance matches the generator internal resistance) is

$$P_{id} = \frac{1}{4}\sigma u^2 B^2 \tag{1}$$

where σ, the electrical conductivity, is

$$\sigma = \frac{n_e e^2}{m_e \nu} \tag{2}$$

and where n_e is the electron number density, e is the unit electric charge, m_e is the electron mass, ν is the electron collision frequency for momentum transfer, u is the gas flow velocity, and B is the magnetic field strength.

Because σ and u are basically independent of B, equation (1) indicates that the optimum power density is obtained at maximum B. However, one finds that in practice the generator performance rapidly deteriorates as the Hall parameter β exceeds approximately unity, where

$$\beta = \frac{eB}{m_e \nu} \tag{3}$$

It is shown in the next section that a reasonable measure of the performance deterioration with β is given by

$$P_{eff} = \frac{1}{4}\sigma u^2 B^2 \frac{1+\beta}{1+\beta^2} \qquad \beta > 1$$

$$P_{eff} = P_{id} \qquad \beta \leq 1 \tag{4}$$

where P_{eff} is the effective power density.

This is the third quantity which will be optimized.

Calculation of Parameters

Effective power density. - Ohm's law, appropriate for an MHD working fluid in the presence of a magnetic field, is, in vector form (ref. 3, eq. 10.56) and for the orientation shown in figure 1,

$$\vec{j} = \sigma(\vec{E} + \vec{u} \times \vec{B}) - \beta \vec{j} \times \hat{b} \tag{5}$$

Equation (5) can be written in component form:

$$j_y + \beta j_x = \sigma(uB + E_y) \tag{6a}$$

$$j_x - \beta j_y = \sigma E_x \tag{6b}$$

where j_x is the Hall current density, j_y is the Faraday current density, E_x is the Hall electric field, and E_y is the Faraday electric field. The power density generated by such a working fluid is

$$P = j_x(-E_x) + j_y(-E_y) \tag{7}$$

MHD generators are built with electrodes segmented in the x direction, and three types of connections are commonly considered (see fig. 2): (1) Faraday, where $j_x = 0$, and for which $E_x = -\beta(uB + E_y)$; (2) diagonal, where $E_y = \varphi E_x$ with $\varphi = \tan \alpha$ where α is the angle the wall segment makes with $\underline{u} \times \underline{B}$; and (3) Hall, where $E_y = 0$.

For each mode equation (7) shows that the power density depends on the value of E_x that it is possible to develop. Equation (6b) shows that the value of E_x for any j_x is proportional to j_y. Since electrode voltage drops limit the current j_y, they will also limit E_x. For a given j_y any current j_x will short out E_x and limit its value. Hence, E_x is a measure of the generator's ability on the one hand to provide j_y and on the other hand to prevent j_x. The quantity

$$K_H(\varphi) = \frac{-E_x}{uB} \frac{1 + \varphi^2}{\varphi + \beta} \tag{8}$$

where E_x is evaluated at the condition $E_y = \varphi E_x$ can be used as a measure of generator performance because it is the fraction of the ideal axial electric field which a

generator attains. As shown in the appendix the power densities of the three types of generators (when loaded so as to give maximum power) are

$$\frac{1 + K_H(0)\beta^2}{1 + \beta^2} \qquad \text{Faraday} \tag{9}$$

$$\frac{P}{\frac{1}{4}\sigma u^2 B^2} = K_H(\varphi)\frac{(\varphi + \beta)^2}{(1 + \varphi^2)(1 + \beta^2)} \qquad \text{Diagonal conducting wall} \tag{10}$$

$$K_H(0)\frac{\beta^2}{1 + \beta^2} \qquad \text{Hall} \tag{11}$$

these results are a generalization of those given in reference 4. These forms allow for internal current leakage and electrode voltage drops by evaluating K_H from experimental results.

The results for K_H from many different experiments are shown in table I. The data are taken from generators with different working fluids as well as different electrode connections. The references from which the data were obtained and, in some cases, the data used in determining K_H are also shown.

The data corresponding to the highest values of K_H are shown in figure 3. Also shown in the empirical relationship

$$\begin{aligned} K_H(\varphi) &= \frac{1}{\beta} \qquad \beta > 1 \\ &= 1 \qquad \beta \leq 1 \end{aligned} \tag{12}$$

which correlates the data with reasonable accuracy.

This correlation agrees with a result obtained in reference 5 for inert gas generators when fluctuations are taken into account. Thus substituting equation (12) for $\beta > 1$ into equation (9) gives

$$P_{eff} = \frac{1}{4}\sigma\frac{1 + \beta}{1 + \beta^2}u^2B^2$$

Then defining

$$\sigma_{eff} \equiv \sigma \frac{1 + \beta}{1 + \beta^2}$$

results in

$$\sigma_{eff}\Big|_{\lim \beta \to \infty} = \sigma \frac{1}{\beta}$$

which is the expression derived in reference 5 (see eq. (19) and fig. 6) for $\beta_{crit} = 1$. Although fluctuations of the type discussed in reference 5 are only predominate in inert-gas, nonequilibrium, MHD generators, it appears that a similar degradation of performance can occur in combustion MHD generators.

Collision frequency for momentum transfer. - To evaluate the conductivity and Hall parameter (eqs. (2) and (3)), we need the electron collision frequency for momentum transfer. This quantity is defined in reference 3 as

$$\nu = \sum_i \nu_{ei} \simeq \sum_i n_i \left(\frac{8kT}{\pi m_e}\right)^{1/2} \langle Q_{ei} \rangle \tag{13}$$

where the sum extends over all species except electrons and where n_i is the number density of the i^{th} species, $\langle Q_{ei} \rangle$ is the momentum transfer cross section between an electron and the i^{th} species, k is the Boltzmann constant, and T is the gas temperature. The quantity $\langle Q_{ei} \rangle$ is calculated from the monoenergetic beam cross section, Q_{ei} (by ref. 6) as

$$\langle Q_{ei} \rangle = \frac{4}{3}\left(\frac{m_e}{2kT}\right)^3 \int_0^\infty Q_{ei}(v) \left[\exp\left(-\frac{\frac{1}{2} m_e v^2}{kT}\right)\right] v^5 \, dv \tag{14}$$

where v is the relative velocity between the collision partners. One of the greatest sources of uncertainty in combustion MHD generator analysis is in the lack of good cross section data in the electron energy range of interest (2000 to 4000 K).

Before proceeding to a discussion of the cross section data used in this report, it is interesting to note the mole fractions of various species in the hydrogen-oxygen-cesium chemistry. These are listed in table II for conditions typical of those analyzed in this report. A discussion of the chemical analysis is presented in the next section. The im-

portant thing to note is that the mole fraction of water (H_2O) is nearly an order of magnitude greater than any of the other species. Furthermore, its cross section is larger than for the other species (as shown in fig. 4), except for cesium which only appears in trace amounts. The result is that the collision frequency is grossly dominated by H_2O. Thus, the only cross section that must be established with some care is that of H_2O.

The value for the monoenergetic cross section for H_2O used in this report was taken from page 9 of reference 7. The momentum transfer cross section obtained by numerical integration of equation (14) is plotted in figure 5 along with the data used by five other researchers in the MHD field. It is seen that there is a wide variation in the values used. The value used in this report is the largest; hence, the results obtained from the optimization of electrical conductivity and power densities are on the conservative side.

Sources of other cross sections used in this report are listed here:

(1) Cesium - Cesium momentum transfer cross section was previously evaluated in reference 6.

(2) Atomic hydrogen (ref. 8, p. 132) - The curve used was an extrapolation of the results of Temkin and Lamkin.

(3) Hydroxyl ion (OH) - A readily available monoenergetic cross section was not found. Therefore, we arbitrarily took a value between the two points given in reference 9 and made the cross-section constant.

(4) Molecular hydrogen - The momentum cross section is given directly in reference 8 (p. 127).

(5) Molecular oxygen - The experimental results given in reference 8 (p. 144) were used.

(6) Atomic oxygen - The curve labeled beam experiment, Bates and Massey, and Lin and Kivel, was used (ref. 8, p. 133).

(7) Ions - The collision frequency given by equation (29) of reference 6 was used.

Method of Solution

The equilibrium chemistry of hydrogen-oxygen-cesium combustion was calculated using the rocket option of reference 10. This program calculates the mole fractions of the 31 species listed in table II as functions of combustion pressure and isentropic expansion ratio. Because collision cross sections were not known for all of the species, the unknown were assigned the cross sections given here:

(1) Cesium cross section - Cs, CsO, CsOH, Cs_2, Cs_2O, $Cs_2O_2H_2$

(2) H_2O cross section - H_2O, HO_2, H_2O_2

(3) H_2 cross section - $\dot{H}_2$

(4) O_2 cross section - O_2, O_3

(5) H cross section - H

(6) O cross section - O

(7) Ion cross section - Cs^+, $CsOH^+$, H^+, H^-, O^+, O^-, OH^+, OH^-, O_2^-

(8) OH cross section - OH

On this basis the conductivity and power densities given by equations (1), (2), and (4) are readily calculable as functions of the following variable parameters:

(1) Seed fraction - 1 part CsOH dissolved in two parts water. The CsOH is introduced into the combustion chamber as a solid dissolved in water (as a liquid). Both were introduced at room temperature. The percent seed is defined as

$$\% \text{ seed} = \frac{\text{Moles } (CsOH + 2H_2O)}{\text{total moles}} 100 \tag{15}$$

(2) Oxygen to hydrogen weight ratio -

$$O/F = \frac{\text{weight of } O_2}{\text{weight of } H_2} \tag{16}$$

The oxygen and hydrogen were introduced into the combustion chamber as room temperature gases.

(3) Combustion chamber pressure - The assigned value of combustion chamber pressure.

(4) Area ratio - The ratio of inlet area of the MHD duct to the throat area of combustor.

(5) Magnetic field - The assigned value of magnetic field strength.

The question investigated in this study is what values of these five parameters should be chosen to optimize the conductivity or the power densities. The range of values studied are seed fraction all values; O/F, 4 to 12; combustion pressure, 0.5 to 4 megapascals; area ratio, ∞ subsonic to 10 supersonic; and magnetic field, 0 to 10 teslas.

The procedure adopted was to investigate the effect of varying one parameter at a time to find an operating value that optimizes the conductivity or power densities over the range of values of the other parameters. This procedure is successful primarily because the optimum values vary slowly as a function of seed fraction, O/F, and Mach number.

RESULTS AND DISCUSSION

Optimum Seed Fraction

The influence of seed fraction on the optimum values of conductivity and power densities is evaluated by plotting conductivity and power densities as a function of seed fraction for various values of one of the other four quantities (O/F, combustion pressure, area ratio, magnetic field) while holding the other three values at an arbitrarily chosen value which is near the midpoint of their range. These fixed values were O/F = 8 (stoichiometric); combustion pressure, 1.03 megapascals, and area ratio, 1.30 (at M = ~1.6). Because conductivity is independent of magnetic field and the ideal power density varies as B^2 (eq. (1)), there is no optimum value as a function of magnetic field for these two parameters. Hence, the influence of seed fraction on magnetic field variation involves only the optimization of the effective power density. This effect differs for low and high values of magnetic field. For low magnetic field (i.e., $\beta \leq 1$) the effective power density (eq. (4)) equals the ideal power density (eq. (1)). Hence, the influence of seed fraction on effective power density at low magnetic field is the same as it is on ideal power density. Therefore, the fixed value of B for all computations of seed effect was set at the upper range of magnetic field, namely, 10 teslas.

Figure 6 shows the results. The only important thing to note is that, except for the curves at the very low value of O/F = 4 shown in figure 6(a) (which these curves show is far below the optimum O/F ratio), there is a slow variation of all three parameters as a function of percent seed. As a result, at approximately 3.5 mole percent seed, all the curves are within a few percentage points of their optimum value. Therefore, a seed fraction of 3.5 percent is chosen as the optimal seed fraction and is used to determine the optimal values of the other parameters.

The power densities optimize in these figures primarily because the conductivity optimizes with increasing seed fraction. This can be readily illustrated for an inert gas containing an ionizable seed. The electron number density n_e is related to the seed number density n_s by Saha's law (ref. 3).

$$n_e \propto \sqrt{n_s} \exp\left(-\frac{T_i}{2T}\right) \tag{17}$$

where T_i is the temperature corresponding to the ionization potential. Ignoring for simplicity electron-ion collisions (weakly ionized gas), we obtain a collision frequency (given by eq. (13)) that is proportional to

$$\nu \propto n_n\langle Q_{en}\rangle + n_s\langle Q_{es}\rangle \tag{18}$$

Substituting equations (17) and (18) into equation (2) shows that the conductivity is proportional to

$$\sigma \propto \frac{\sqrt{n_s}\, \exp\left(-\frac{T_i}{2T}\right)}{n_n\langle Q_{en}\rangle + n_s\langle Q_{es}\rangle} \tag{19}$$

At low seed fractions ($n_n\langle Q_{en}\rangle >> n_s\langle Q_{es}\rangle$) the conductivity increases as the square root of the seed fraction. The equation reaches a maximum when $n_n\langle Q_{en}\rangle = n_s\langle Q_{es}\rangle$. A more detailed study of this effect in inert gas systems is contained in reference 11.

In the combustion MHD system considered here, the location of the maximum is not as straightforward since it is masked by the chemistry. In addition the alkali metal seed is introduced in the form of CsOH dissolved in water, and the water acts as a diluent which decreases the gas temperature. From equation (19) this obviously results in a decrease in conductivity and hence also in power density.

Optimum Oxygen-Hydrogen Ratio

Having set the optimum seed fraction at 3.5 percent we now proceed to optimize the O/F. The magnetic field remains fixed at 10 tesla as discussed in the previous section. The two remaining variables are the combustion pressure and area ratio. In figure 7 conductivity and the power densities are plotted as functions of O/F with area ratio as a parameter for three combustion pressures. In these nine figures all the curves are within 10 percent (and most are within a few percent) of their maximum at an O/F of approximately 7.5. Therefore, an O/F of 7.5 is chosen as the optimal O/F and is used to determine the optimal values of the other parameters.

As before, the power densities show an optimum in these figures primarily due to the influence of O/F on the conductivity. On either the fuel rich or oxygen rich side of stoichiometric (O/F = 8) there is a surplus of particles that have nothing with which to react and hence act as a diluent and decrease the temperature and hence the conductivity (eq. (19)). However, the conductivity plots of figure 7 indicate that the peak in the conductivity occurs on the fuel rich side of stoichiometric. This is due to the chemistry of the system and occurs because cesium is a strong reducing agent. Therefore, as O/F increases an increasingly greater amount of CsOH and CsO is formed. This results in less atomic cesium, which produces the ionization, and thus results in a lower free electron density and hence in a lower conductivity.

Optimum Mach Number

With the optimum seed fraction set at 3.5 percent and O/F at 7.5, we now investigate the influence of area ratio (or equivalently the influence of Mach number) on the optimum values of conductivity and power densities. From the conductivity plot of figures 6(c) and 7, it is obvious that the conductivity decreases with increasing Mach number and is therefore a maximum in the combustion chamber (where M = 0). This is due to the strong temperature dependence of the conductivity.

In figure 8 σu^2 (which is proportional to ideal power density) is plotted versus Mach number for various combustion pressures. The maximum occurs at a Mach number of approximately 2.5. The Mach number for maximum power density shows only a slight decrease with increasing combustion pressure. The maximum occurs as a result of the interplay between the rapidly decreasing value of conductivity and the increasing value of velocity with Mach number.

Also in figure 8 the effective power density P_{eff} is plotted versus Mach number for various combustion pressures. The maximum values of power density for the various pressures form a locus such that a maximum value of effective power density occurs for a chamber pressure between 1 and 20 megapascals. The effect of pressure is discussed in greater detail in the next two sections.

Optimum Combustion Pressure

The conductivity plots of figures 6(b) and 7 show that the maximum conductivity occurs at the lowest combustion pressure. This results from the fact that the temperature is only slightly affected by combustion pressure for the pressure range considered herein so that for the same seed fraction equation (19) reduces to

$$\sigma \propto \frac{\exp\left(\frac{T_i}{2T}\right)}{\sqrt{p}} \tag{20}$$

that is, the conductivity decreases approximately as the inverse square root of the pressure. The σu^2 plots of figures 6(b) and 7 indicate that the ideal power density follows a similar trend, due to the fact that the velocity is only slightly affected by combustion pressure. Hence the ideal power density depends on combustion pressure only through the conductivity.

For high combustion pressure ($\beta < 1$) the effective power density reduces to the ideal power density. The power density decreases with increasing combustion pressure as does the conductivity. For the constant area ratio case of figure 6(a) (top plot) the

temperature is only slightly affected by combustion pressure. Therefore, from equations (3), (13), and (18) the Hall parameter is approximately proportional to

$$\beta \propto \frac{B}{p} \tag{21}$$

Hence as $\beta \to \infty$ from equations (4), (20), and (21) yield

$$P_{eff} \propto \sqrt{p} \tag{22}$$

and for $\beta \gg 1$, the effective power density increases with increasing combustion pressure. Therefore, the effective power density goes through a maximum with increasing combustion pressure for a given magnetic field strength (shown in figs. 6(b) (bottom plot) and 8). Figure 8 also shows that the Mach number for optimum effective power density decreases with decreasing combustion pressure. Since for a given combustion pressure the static pressure in the MHD channel is determined by the Mach number, this result indicates that there probably is an optimum static pressure for a given magnetic field strength. Or conversely, for a given magnetic field strength there is an entrance static pressure and hence combustion pressure and Mach number which optimizes the effective power density.

Maximum Effective Power Density and Its Consequences

As noted from figure 8 the maximum values of P_{eff} for various combustion pressures form a locus of points such that a maximum value occurs as a function of combustion pressure. This is a consequence of the empirical correlation of figure 3. For the magnetic field strength of 10 teslas used, this maximum occurs between combustion pressures of 1 and 2 megapascals. It also may be noted that this maximum value then sets the Mach number at which one should operate. It is therefore concluded that magnitude of the magnetic field strength sets the combustion pressure and Mach number at the entrance of the MHD generator for maximum effective power density.

The optimum combustion pressure and Mach number for maximum effective power density are plotted versus magnetic field strength in figures 9 and 10. The optimum combustion pressure increases nearly in direct proportion to the magnetic field strength, and the Mach number is nearly constant at a value of 2. The static pressure corresponding to these operating combustion pressures and Mach numbers is plotted in figure 11 as a function of magnetic field strength. This static pressure is nearly proportional to the magnetic field strength which indicates that the maximum effective power density should occur at nearly constant β (see eq. (21)).

This observation is confirmed by the plot shown in figure 12, wherein β at the operating conditions of figures 10 and 11 is plotted versus magnetic field. That β for maximum power density is constant at a value of 1 should not be totally unexpected. The gas temperature and velocity for a given expansion Mach number are relatively insensitive to combustion pressure. Since the optimum Mach number is relatively constant with operating conditions, that is, magnetic field, it follows that the gas temperature and velocity are relatively insensitive to operating conditions. Therefore, for a given value of magnetic field the conductivity from equation (20) is proportional to

$$\sigma \propto \frac{1}{\sqrt{p}}$$

and the Hall parameter from equation (21) is proportional to

$$\beta \propto \frac{1}{p} \tag{23}$$

Therefore,

$$\sigma \propto \sqrt{\beta} \tag{24}$$

Substituting equations (23) and (24) into equation (4), we find that the effective power density is proportional to

$$P_{eff} \propto \sqrt{\beta}\,\frac{1+\beta}{1+\beta^2} \tag{25}$$

Maximizing equation (25) with respect to β, we find that β must satisfy

$$\frac{1}{2}+\frac{3}{2}\beta-\frac{3}{2}\beta^2-\frac{1}{2}\beta^3=-(\beta-1)\left(\frac{1}{2}\beta^2+2\beta+\frac{1}{2}\right)=0 \tag{26}$$

Equation (21) is satisfied when $\beta = 1$. (The other two roots are negative.) The value $\beta = 1$ is a function of the empirical model chosen (see eq. (12)). If a different expression had been chosen, β would take on a different optimum value.

Additional calculations were made to evaluate the variation of the maximum effective power density with magnetic field strengths. The results are shown in figure 13. The effective power density increases monotonically with magnetic field, as does the ideal power density. The corresponding open circuit voltage uB is plotted versus magnetic field in figure 14.

CONCLUDING REMARKS

In this study we have determined the values of percent seed, oxygen to fuel ratio, combustion pressure, Mach number, and magnetic field which optimize the values of either conductivity or power densities at the entrance of an MHD generator using a cesium seed hydrogen-oxygen working fluid. Although the utilization of these values as operating parameters for an MHD generator should result in the shortest length device, it is not clear how these results would be affected by percent power extraction and power level of the device. These questions are currently being investigated.

SUMMARY OF RESULTS

The determinations of near optimum operating conditions for a hydrogen-oxygen, cesium-seeded MHD power generator have been shown based on the maximization of either electrical conductivity or power density at the entrance of the generator. Two forms of the power density were investigated. The first was the ideal value derived from theory and the second was an effective value based on an empirical formula obtained from the analysis of a broad range of experimental data.

The conductivity and power densities maximize within a narrow range of molar seed fractions and oxygen to fuel weight ratios. However, within the range of conditions investigated (percent seed 0 to 10; O/F = 4 to 12; combustion pressure, 0.517 to 4.14 mPa; Mach 0.5 to 3) the conductivity and power densities are slowly varying with percent seed and oxygen to fuel ratio so that the near maximum values of conductivity and power densities occurred at 3.5 percent seed and an oxygen to fuel ratio of 7.5. Therefore, these values appear to be the near optimum operating conditions for percent seed and O/F ratio.

Using these values of percent seed and oxygen to fuel ratio the effect of Mach number, combustion pressure, and magnetic field strength upon the optimum values of conductivity and power densities was investigated. The maximum electrical conductivity was found when the gas is at the combustion temperature or at $M = 0$. This reflects the strong temperature, that is, free electron density, dependence of the conductivity. Since the temperature is highest at $M = 0$ so is the conductivity. The ideal power density maximum occurred at $M \simeq 2.5$ nearly independent of combustion pressure. Since the ideal power density P_{id} is proportional to σu^2, the maximum occurs as a trade-off between the rapid increase in velocity with Mach number and the decrease of conductivity due to decreasing temperature with Mach number. Both the conductivity and ideal power density were monotonic decreasing functions of increasing combustion pressure. In both cases this is due to the nearly inverse, square root dependence of conductivity on pressure. For the transport theory formulation of the conductivity used in this report, the

conductivity is independent of magnetic field while the ideal power density increases with the square of the magnetic field.

The optimum values of the effective power occurred at strongly coupled values of Mach number, combustion pressure, and magnetic field strength. These quantities optimized the effective power density such that the Hall parameter was unity. This result is sensitive to the empirical correlation chosen.

Lewis Research Center,
National Aeronautics and Space Administration,
Cleveland, Ohio, August 18, 1976,
506-25.

APPENDIX - EFFECTIVE POWER DENSITY FOR VARIOUS ELECTRODE CONFIGURATIONS

MHD generators can be viewed as two coupled generators with equivalent circuits for Faraday and Hall connections:

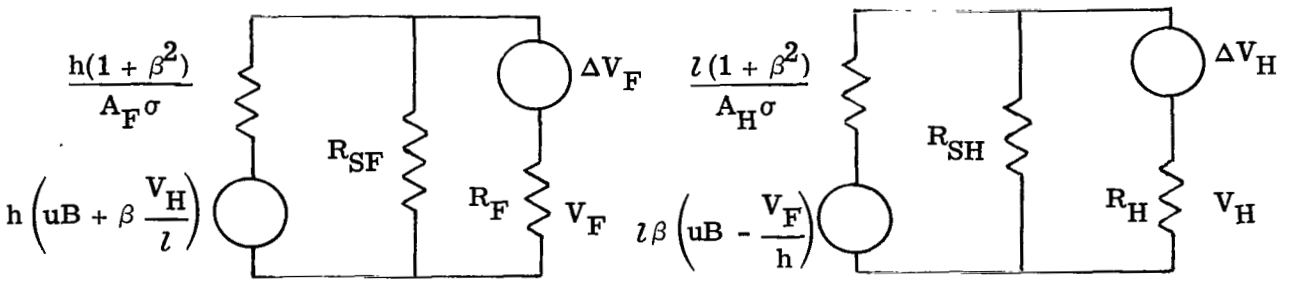

where h is the distance between Faraday electrodes and l is the distance between Hall electrodes. The conducting cross section area is A, resistances R, the voltage V, and the current I. The subscripts correspond to Hall H and Faraday F generators. These equivalent circuits can, in turn, be replaced by a second pair of equivalent circuits:

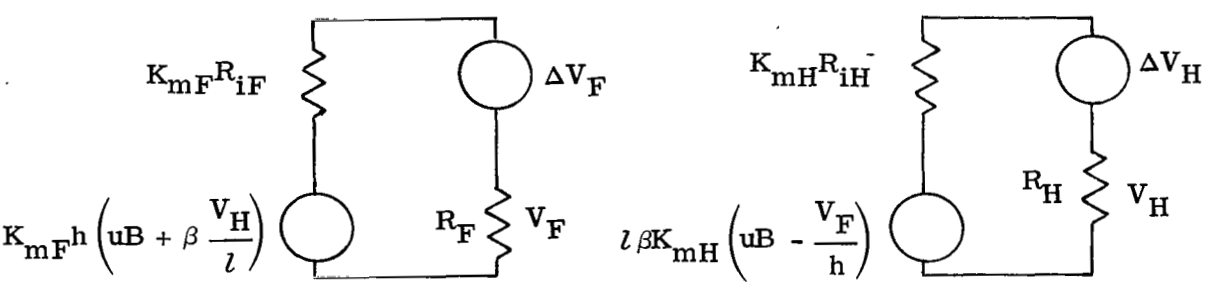

where

$$K_{mF} = \frac{R_{SF}}{R_{SF} + R_{iF}} \qquad K_{mH} = \frac{R_{SH}}{R_{SH} + R_{iH}}$$

$$R_{iF} = \frac{h(1+\beta^2)}{A_F\sigma} \qquad R_{iH} = \frac{l(1+\beta^2)}{A_H\sigma}$$

These coupled voltage equations for each generator are

$$K_{mF}h\left(uB + \beta\frac{V_H}{l}\right) - (V_F + \Delta V_F) = \frac{K_{mF}R_{iF}}{R_F}V_F \tag{A1}$$

$$K_{mH}l\beta\left(uB - \frac{V_F}{h}\right) - (V_H + \Delta V_H) = \frac{K_{mH}R_H}{R_H}V_H \tag{A2}$$

The load voltages for the generators can be determined by solving these equations:

$$\frac{V_H}{luB\beta} = \frac{\left(1 + K_{mF}\frac{R_{iF}}{R_F}\right)\left(K_{mH} - \frac{\Delta V_H}{luB\beta}\right) - K_{mH}\left(K_{mF} - \frac{\Delta V_F}{huB}\right)}{\left(1 + K_{mF}\frac{R_{iF}}{R_F}\right)\left(1 + K_{mH}\frac{R_{iH}}{R_H}\right) + K_{mF}K_{mH}\beta^2} \tag{A3}$$

$$\frac{V_F}{huB} = \frac{\left(1 + K_{mH}\frac{R_{iH}}{R_H}\right)\left(K_{mF} - \frac{\Delta V_F}{huB}\right) + K_{mF}\beta^2\left(K_{mH} - \frac{\Delta V_H}{luB\beta}\right)}{\left(1 + K_{mF}\frac{R_{iF}}{R_F}\right)\left(1 + K_{mH}\frac{R_{iH}}{R_H}\right) + K_{mF}K_{mH}\beta^2} \tag{A4}$$

It is now possible to derive expressions for the power density for two types of generators.

First, consider a generator with the condition $R_H \to \infty$. This is called a Faraday generator. In this case there is no current flowing in the Hall load resistance, and the Faraday voltage is

$$\frac{V_F}{huB} = \frac{K_{mF} - \frac{\Delta V_F}{huB} + K_{mF}\left(K_{mH} - \frac{\Delta V_H}{luB\beta}\right)\beta^2}{1 + K_{mF}\frac{R_{iF}}{R_F} + K_{mF}K_{mH}\beta^2} \tag{A5}$$

The maximum power occurs when the load resistance R_F is

$$R_F = \frac{K_{mF}R_{iF}}{1 + K_{mF}K_{mH}\beta^2} \tag{A6}$$

For this loading of the generator, the generator power density is

$$P = \frac{1}{4}\sigma u^2 B^2 \frac{\left[K_{mF} - \frac{\Delta V_F}{huB} + K_{mF}\left(K_{mH} - \frac{\Delta V_H}{\ell u \beta B}\right)\beta^2\right]^2}{K_{mF}\left(1 + K_{mF}K_{mH}\beta^2\right)(1 + \beta^2)} \tag{A7}$$

Second, consider a generator with the condition $R_F = 0$. This is called a Hall generator. Since there is no voltage across the Faraday load resistance, the power is generated entirely in the Hall circuit, and the Hall voltage is

$$\frac{V_H}{\ell u B \beta} = \frac{K_{mH} - \frac{\Delta V_H}{\ell u \beta B}}{1 + K_{mH}\left(\frac{R_{iH}}{R_H}\right)} \tag{A8}$$

The maximum power occurs when the load resistance R_H is

$$R_H = K_{mH}R_{iH} \tag{A9}$$

The power density for this generator loading is

$$P_H = \frac{1}{4}\sigma u^2 B^2 \frac{\left(K_{mH} - \frac{\Delta V_H}{\ell u \beta B}\right)^2 \beta^2}{K_{mH}(1 + \beta^2)} \tag{A10}$$

The diagonal conducting wall generator can be analyzed by using one equivalent circuit:

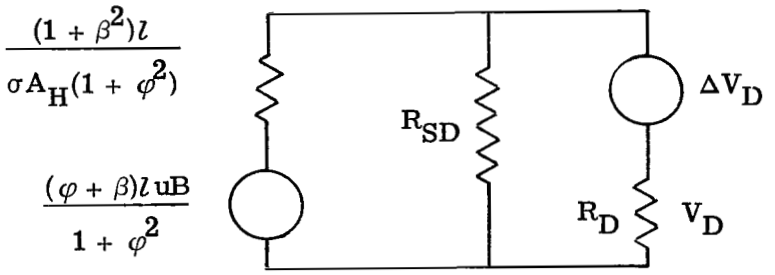

which, in turn, can be written as

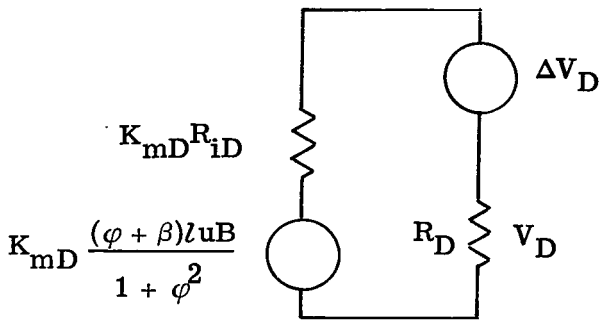

where

$$K_{mD} = \frac{R_{SD}}{R_{SD} + R_{iD}}$$

$$R_{iD} = \frac{(1+\beta^2)\ell}{\sigma(1+\varphi^2)A_D}$$

The load voltage is

$$V_D = \frac{K_{mD}\left(\frac{\varphi+\beta}{1+\varphi^2}\right)\ell uB - \Delta V_D}{1 + K_{mD}\left(\frac{R_{iD}}{R_D}\right)} \tag{A11}$$

The maximum power occurs when the load resistance is $R_D = K_{mD}R_{iD}$, and the power density becomes

$$P_D = \frac{1}{4}\sigma u^2 B^2 \frac{\left[K_{mD} - \frac{\Delta V_D}{\ell uB\left(\frac{\varphi+\beta}{1+\varphi^2}\right)}\right]^2}{K_{mD}} \frac{(\varphi+\beta)^2}{(1+\varphi^2)(1+\beta^2)} \tag{A12}$$

If electrode drops are negligible, then the power density divided by the ideal power density is

$$\frac{P}{\frac{1}{4}\sigma u^2\beta^2} = \begin{cases} K_{mF}\dfrac{1 + K_{mH}\beta^2}{1 + \beta^2} & \text{Faraday} \\ \dfrac{K_{mH}\beta^2}{1 + \beta^2} & \text{Hall} \\ K_{mD}\dfrac{(\varphi + \beta^2)}{(1 + \varphi^2)(1 + \beta^2)} & \text{Diagonal conducting wall} \end{cases}$$

Even though K_{mH} and K_{mD} are defined in terms of resistances, they can be evaluated from the voltage measurements (eq. (A3)).

$$\frac{V_H}{\ell u\beta B} = K_{mH}$$

when $R_F = 0$ and for the diagonal conducting wall (eq. (A11))

$$\frac{V_D(1 + \varphi^2)}{\ell uB(\varphi + \beta)} = K_{mD}$$

Thus, if

$$K_H(\varphi) = \frac{(-Ex)}{uB}\left(\frac{1 + \varphi^2}{\varphi + \beta}\right)$$

where it is understood that $E_y = \varphi E_x$ and K_{mF} is set equal to 1, although all of the power densities can be expressed in terms of $K_H(\varphi)$ as

$$\frac{P}{\frac{1}{4}\sigma u^2 B^2} \approx \begin{cases} \dfrac{1 + K_H(0)\beta^2}{1 + \beta^2} & \text{Faraday} \\ \dfrac{K_H(0)\beta^2}{1 + \beta^2} & \text{Hall} \\ \dfrac{K_H(\varphi)(\varphi + \beta)^2}{(1 + \beta^2)(1 + \varphi^2)} & \text{Diagonal conducting wall} \end{cases}$$

REFERENCES

1. Gregory, Derek P.: The Hydrogen Economy. Scien, Amer., vol. 228, no. 1, Jan. 1973, pp. 13-21.
2. Carter, C.; and Heywood, J. B.: Optimization Studies on Open-Cycle MHD Generators. Proc. IEEE, vol. 56, no. 9, Sept. 1968, pp. 1409-1419.
3. Sutton, George W.; and Sherman, Arthur: Engineering Magnetohydrodynamics. McGraw-Hill Book Co., Inc., 1965.
4. Celínski, Z. N.: Electrical Equivalent Circuits of DC MHD Generators. Proc. of the Symp. on Magnetohydrodynamic Electrical Power Generation. vol. 1, Int. Atomic Energy Agency 1966, pp. 323-331.
5. Solbes, A.: Instabilities in Non-Equilibrium MHD Plasmas, A. Review. AIAA Paper 70-40, Jan. 1970.
6. Heighway, John E.; and Nichols, Lester D.: Brayton Cycle Magnetohydrodynamic Power Generation with Nonequilibrium Conductivity. NASA TN D-2651, 1965.
7. Brown, Sanborn C.: Basic Data of Plasma Physics. John Wiley & Sons, Inc., 1959.
8. McDaniel, Earl W.: Collision Phenomena in Ionized Gases. John Wiley & Sons., Inc., 1964.
9. Mori, Y., et al.: Experimental Study on Electrical Conductivity of Combustion Gas Plasma and Phenomena Near Electrode. Fifth Int. Conf. on Magnetohydrodynamic Power Generation. vol. I, Int. Atomic Energy Agency, 1971, pp. 11-26.
10. Gordon, Sanford; and McBride, Bonnie J.: Computer Program for Calculation of Complex Chemical Equilibrium Compositions, Rocket Performance, Incident and Reflected Shocks, and Chapman-Jonguet Detonations. NASA SP-273, 1971.
11. Smith, J. Marlin; and Shair, F. H.: Theoretical Optimum Seed Concentrations in Slightly Ionized Nonequilibrium Plasmas. Phys. Fluids, vol. 9, no. 8, Aug. 1956, pp. 1615-1617.
12. Wu, Y. C. L.; et al.: Two-Terminal Connected Open Cycle MHD Generators. Ninth Symposium on Engineering Aspects of Magnetohydrodynamics. Univ. of Tennessee Space Inst., 1968, pp. 85-98.
13. DeMontardy, A.; and Pericart, J.: Electrical Performance of a Duct with Segmented Electrodes Under Various Conditions. Proc. IEEE, vol. 56, no. 9, Sept. 1968, pp. 1547-1555.
14. Teno, J.; et al.: Hall Configuration MHD Generator Studies. Proc. of the Symp. on Electricity from MHD. vol. III, Int. Atomic Energy Agency, 1966, pp. 603-614.

15. Sonju, O. K.; Teno, J.; and Brogan, T. R.: Comparison of Experimental and Analytical Results for a 20-MW, Combustion-Driven, Hall Configuration MHD Generator. Eleventh Symp. on Engineering Aspects of Magnetohydrodynamics. D. G. Elliott, ed., California Institute of Technology, 1970, pp. 5-10.

16. Dicks, J. B.; et al.: Continuation of Diagonal Conducting Wall Generator Research. Tenth Symp. on Engineering Aspects of Magnetohydrodynamics. M.I.T, 1969, pp. 183-193.

17. Wu, Y. C. L.; et al.: Theoretical and Experimental Studies of MHD Power Generation with Char. Twelfth Symp. on Engineering Aspects of Magnetohydrodynamics. Argonne National Laboratory, 1972, pp. II. 1. 1 - II. 1. 14.

18. Holt, J. F.; et al.: Experiments with the KIVA-1 Open Cycle MHD Generator System. Thirteenth Symp. on the Engineering Aspects of Magnetohydrodynamics. Stanford Univ., 1973, pp. II.2.1-II.2.7.

19. Mori, Y.; et al.: Experiments on MHD Generation with ETL Mark II. Proc. of the Symp. on Electricity from MHD. vol. IV, Int. Atomic Energy Agency 1968, pp. 2761-2768.

20. Mattsson, A. C. J.; et al.: Energetics 6: Magnetohydrodynamics Power. Mech. Eng., vol. 88, no. 11, Nov. 1966, pp. 38-41.

21. Louis, J. F.; Lothrop, J.; and Brogan, T. R.: Fluid Dynamic Studies with a Magnetohydrodynamic Generator. Phys. Fluids, vol. 7, no. 3, Mar. 1964, pp. 362-374.

22. Bertolini, E.; et al.: Closed Cycle MHD Subsonic Power Generation Experiments at Frascati. Thirteenth Symposium on the Engineering Aspects of Magnetohydrodynamics. Stanford Univ., 1973, pp. I. 1. 1-I. 1. 11.

23. Miyata, M.: Effects of J×B Force on the Shock Tube Driven Nonequilibrium Faraday Generator. Thirteenth Symp. on the Engineering Aspects of Magnetohydrodynamics. Stanford Univ., 1973, pp. I. 5. 1-I. 5. 6.

24. Shioda, S.; et al.: Experiments in a Faraday MHD Generator with a Supersonic Seeded Helium Flow within a Relaxation Region. Twelfth Symp. on the Engineering Aspects of Magnetohydrodynamics. Argonne National Laboratory, 1972, pp. I.7.1-I.7.10.

25. Bertoline, E.; et al.: Closed Cycle MHD Experiments with a Large Blow Down Facility. Ninth Symp. on the Engineering Aspects of Magnetohydrodynamics. Univ. of Tenn. Space Institute 1968, pp. 130-141.

26. Decher, Reiner; and Kerrebrock, Jack L.: Electrode Wall - End Loop Shorting in a Non-equilibrium MHD Generator. 9th Symp. on the Engineering Aspects of Magnetohydrodynamics. Univ. of Tennessee Space Institute, 1968, pp. 142-155.

27. Zauderer, Bert.; and Tate, Eric.: Electrical Characteristics of a Linear, Non-Equilibrium, MHD Generator. Proc. IEEE, vol. 56, no. 9, Sept. 1968, pp. 1535-1547.

28. Zauderer, B.; and Tate, E.: Experiments in a Large Non-Equilibrium MHD Generator with Cesium Seeded Noble Gases and Heated Electrodes. Fifth Int. Conf. on Magnetohydrodynamic Power Generation. vol. II, Int. Atomic Energy Agency, 1971, pp. 431-446.

29. Buznikov, A. E.; et al.: Experimental Investigations of Influence of Boundary Layers upon the Performance of MHD Generator Within a Wide Range of Hall Parameters. Fifth Int. Conf. on Magnetohydrodynamic Power Generation. vol. I, Int. Atomic Energy Agency, 1971, pp. 335-350.

30. Nichols, Lester D.; and Sovie, Ronald J.: Hall Current Effects in the Lewis MHD Generator. NASA TM X-2606, 1972.

31. Keuhne, W. D.; and Kolb, G.: Angewandte Magnetohydrodynamik-Heft 9. Berechnung der Kenngrossen von Arbeitsgasen des MHD-Verbrennungsgas-Generators (Applied Magnetohydrodynamics. Vol. 9 - Calculation of the Characteristic Quantity of the Working Gas of the MHD-Combustion Gas Generator). JUL-874-TP, Institut fur Technische Physik (Julich, West Germany), 1972.

32. Gaponov, I. M.; et al.: Electric Conductivity of a Plasma Composed of Natural Gas Combustion Products Seeded With Potash. High Temp., vol. 10, no. 5, 1973, pp. 992-993.

33. Rosa, Richard J.: Magnetohydrodynamic Energy Conversion. McGraw-Hill Book Co., Inc., 1968.

34. Raeder, J.; and Bünde, R.: Basic Equations and Fundamental Data for Combustion MHD Generators. Max-Planck IPP-IV-60, Institute for Plasmaphysics, Garching (West Germany), 1973.

TABLE I. - EXPERIMENTAL DATA FOR CALCULATION OF GENERATOR COEFFICIENT

Generator type	Reference	Hall parameter, β	Hall electric field, $-E_x$ volt/M	Gas flow velocity, u M/sec	Magnetic field strength, B Tesla	Tan α[a], φ	Generator coefficient $K_H(\varphi)$
Combustion	12	1.45	772	1630	1.9	0	0.172
	13	1.10	443	641	2.5	↓	.246
	14	4.15	3360	2250	3.1		.116
	15	2.8	(b)	2250	1.9	↓	[b].271
	16	1.45	1480	1630	1.9	.578	.319
	17	2.7	1580	1000	2.2	1.0	.39
	18	1.3	4000	2500	1.9	1.0	.725
	19	2.4	1210	1000	3.4	0	.148
	20	1.7	1250	1400	2.4	0	[c].38
	21	1.9	(d)	720	3.3	0	[d].43
Inert gas	22	2.9	4560	1430	3.7	0	0.297
	23,24	4.0	4300	4500	1.13	↓	.211
	25	1.1	700	1050	.65		.93
	↓	1.15	940	1030	1.03		.77
		2.0	1750	1030	1.78		.47
		2.4	2430	1030	2.72		.36
		2.3	1780	1050	1.35		.54
		3.85	2430	1050	2.26		.28
	↓	5.0	2540	1050	2.94		.17
	26	5.1	1030	3600	1.4		.04
	27	3.9	620	985	2.2		.073
	28	4.5	750	1140	1.4		.105
	29	2.8	----	----	----		.234
		5.0	----	----	----		.140
	30	2.3	45	215	.19		.472
		4.2	88	215	.34	↓	.289

[a]See fig. 2 for definition of α.

[b]$K_H(0) = \dfrac{1}{1 - \dfrac{j_x}{\sigma E_x}(1 + \beta^2)}$.

[c]$K_H = \dfrac{-E_x}{(uB + E_y)}$.

[d]$K_H = \left[\dfrac{(1 + \beta^2)P}{\frac{1}{4}\sigma u^2 B^2} - 1\right]\dfrac{1}{\beta^2}$.

TABLE II. - MOLE FRACTIONS FOR STOICHIOMETRIC HYDROGEN AND OXYGEN COMBUSTION WITH CESIUM SEED

[Seed: 4% CsOH/2 moles H_2O.]

Species[a]	Chamber	Throat	Exit	Exit	Exit
	Pressure, N/m^2				
	1.034×10^6	6.006×10^5	2.811×10^5	1.396×10^4	6.370×10^4
	Temperature, K				
	3320	3178	2992	2832	2663
	Mach number				
	0	1.0000	1.5820	1.9993	2.4085
	Mole fractions				
Cs	0.00322	0.00344	0.00373	0.00397	0.00419
Cs^+	.00032	.00030	.00027	.00023	.00019
CsO	.00023	.00019	.00014	.00011	.00007
CsOH	.01327	.01337	.01350	.01363	.01381
E	.00024	.00023	.00022	.00020	.00018
H	.04222	.03671	.02946	.02330	.01706
HO_2	.00006	.00004	.00002	.00001	.00001
H_2	.12461	.11562	.10259	.09017	.07587
H_2O	.66213	.69146	.73199	.76861	.80849
H_2O_2	.00001	.00001	0	0	0
O	.01911	.01617	.01244	.00943	.00655
O^-	.00001	.00001	0	0	0
OH	.09388	.08353	.06961	.05747	.04477
OH^-	.00008	.00006	.00004	.00003	.00002
O_2	.04059	.03885	.03597	.03283	.02880

[a]Additional species considered but whose mole fractions were less than 5×10^{-6} Cs(S), Cs(L), CsOH(S), CsOH(L), $CsOH^+$, Cs_2, Cs_2O, $Cs_2O_2H_2$, H^+, H^-, H_2O(S), H_2O(L), O^+, OH^+, O_2^-, O_3.

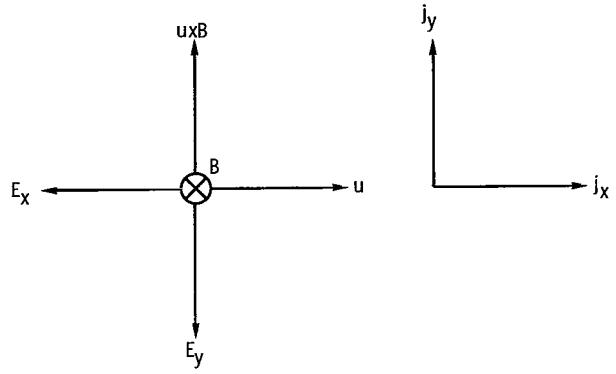

Figure 1. - Coordinates for Ohm's Law.

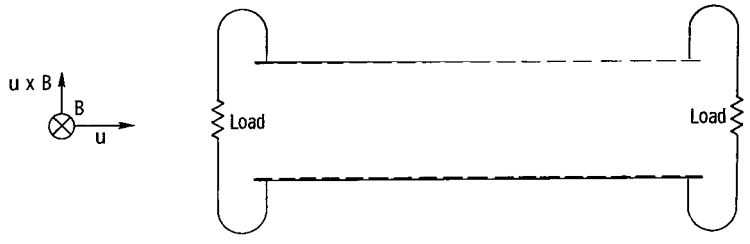

(a) Faraday; load resistances on all electrode pairs; $j_x = 0$, $\tan \alpha = 0$.

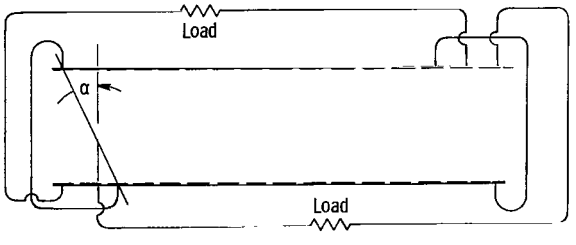

(b) Diagonal; shorted electrode pairs make angle α; $E_y = E_x \tan \alpha$.

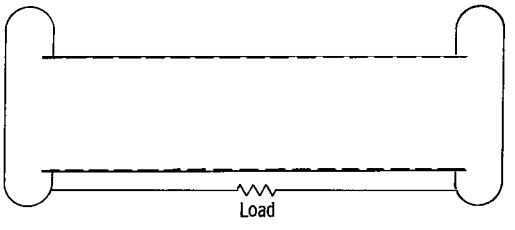

(c) Hall; each electrode pair shorted; $E_y = 0$, $\tan \alpha = 0$.

Figure 2. - Types of generator.

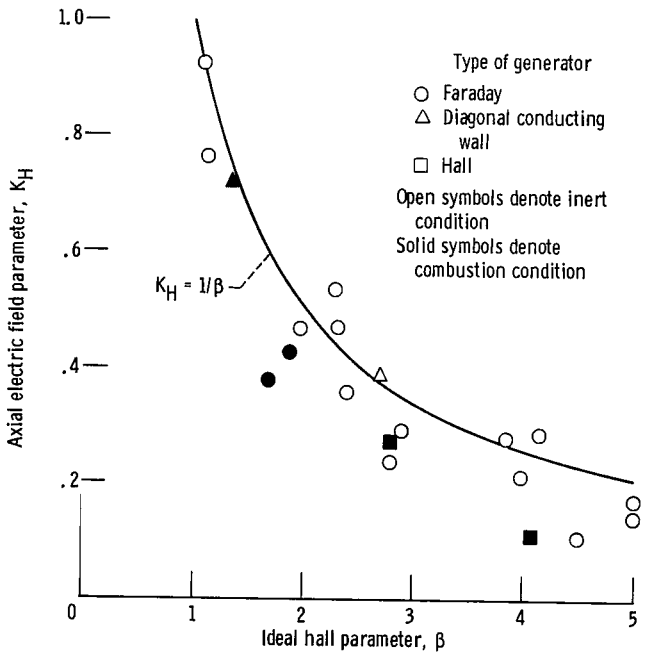

Figure 3. - Best apparent hall parameter data.

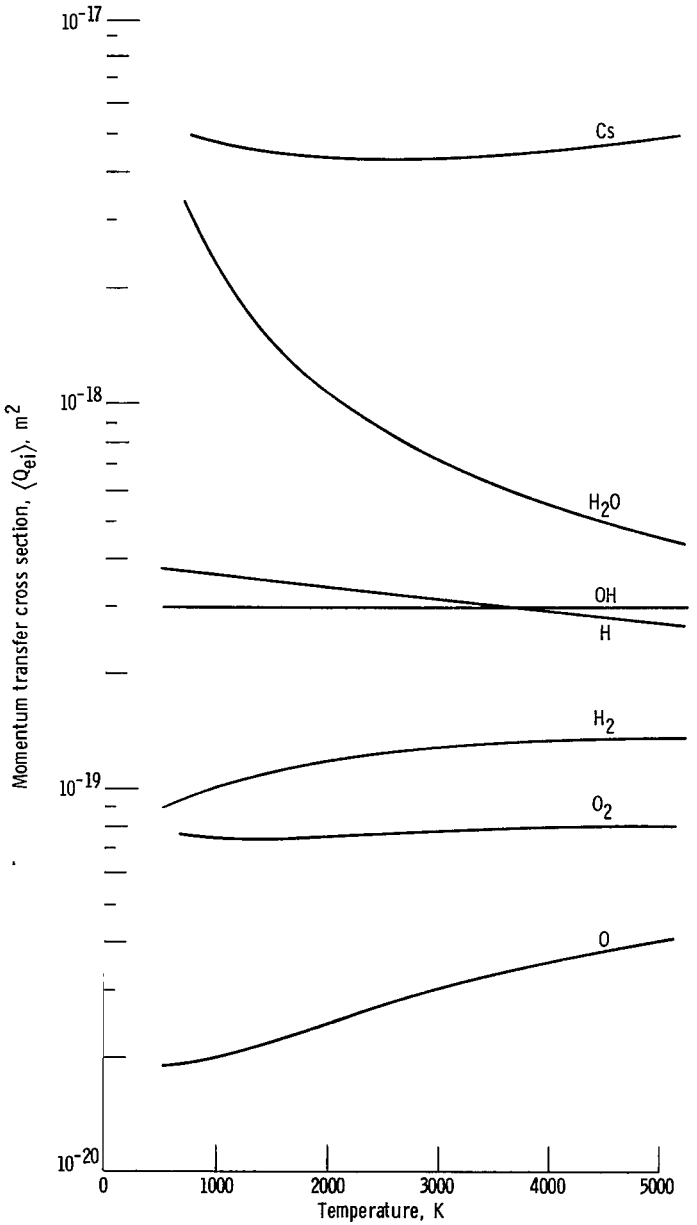

Figure 4. - Cross sections for momentum transfer.

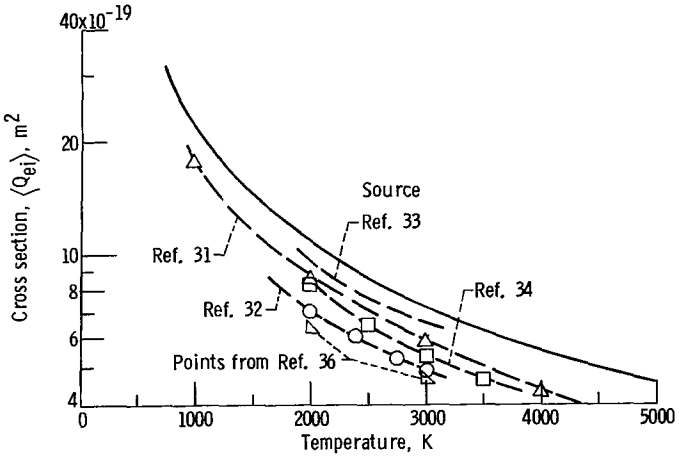

Figure 5. - Comparison of water cross sections used by various researchers in MHD field.

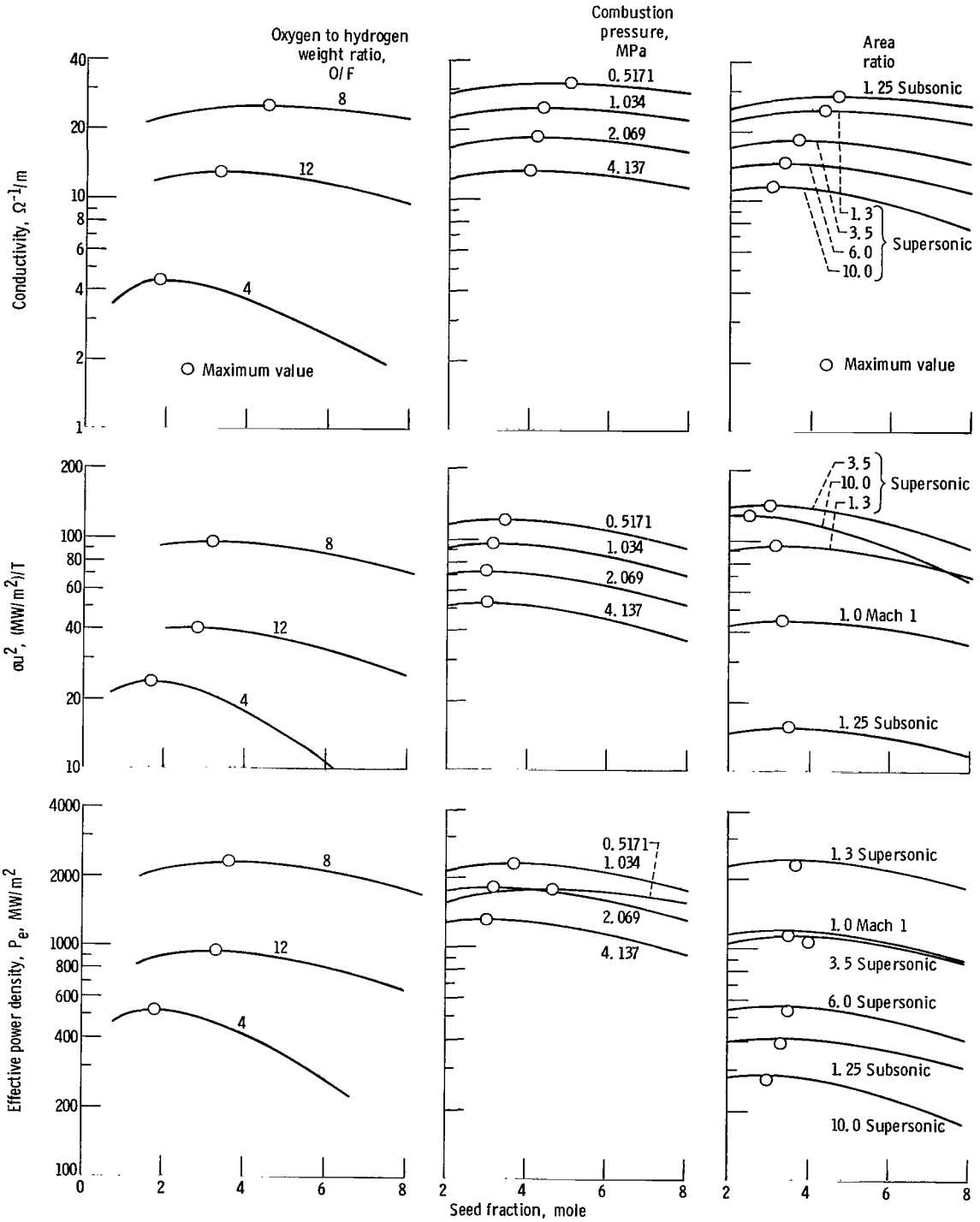

(a) Area ratio, 1.3; combustion pressure, 1.034 megapascals.

(b) Area ratio, 1.3; oxygen to hydrogen weight ratio, 8.

(c) Oxygen to hydrogen weight ratio, 8; combustion pressure, 1.034 megapascals.

Figure 6. - Influence of percent seed on optimum values of conductivity and power densities. Magnetic field strength (applicable to P_e plots only; see text), 10 tesla.

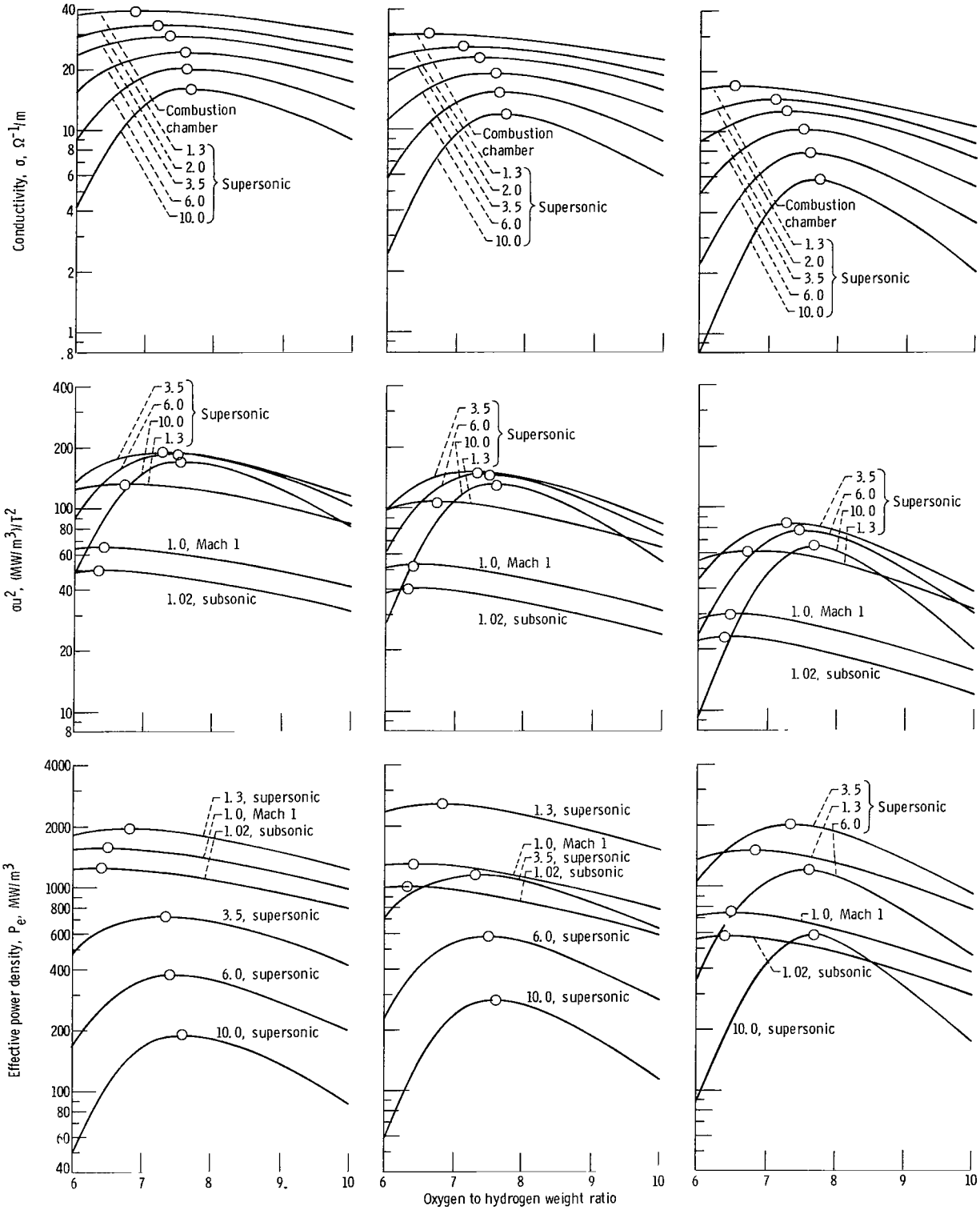

(a) Combustion pressure, 0.5171 megapascals. (b) Combustion pressure, 1.034 megapascals. (c) Combustion pressure, 4.137 megapascals.

Figure 7. - Influence of oxygen to hydrogen weight ratio on conductivity and power densities. Seed fraction, 3.5 mole percent; magnetic field strength (applicable to P_ϵ plots only), 10 teslas.

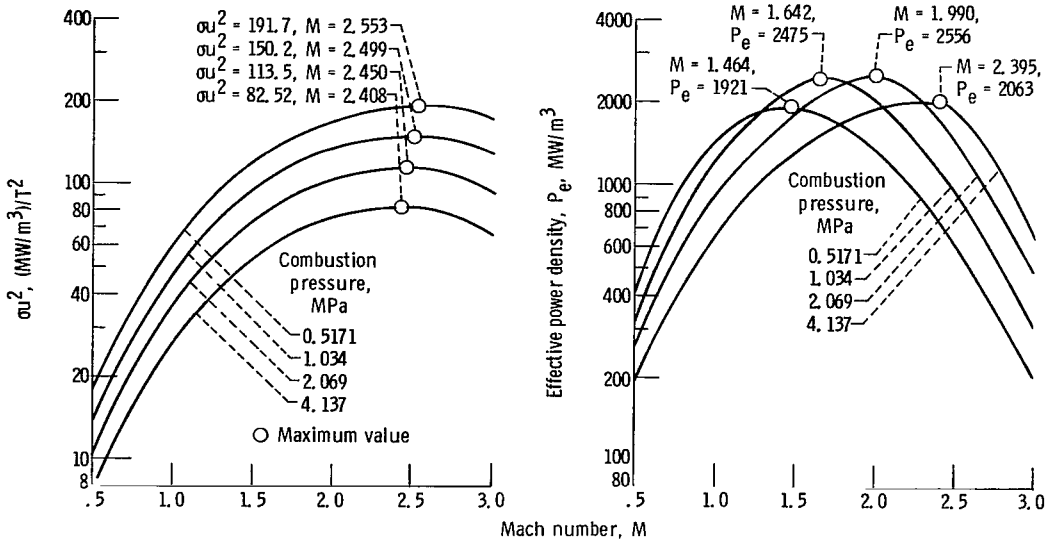

Figure 8. - Influence of Mach number on power densities. Seed fraction, 3.5 mole percent; oxygen to hydrogen weight ratio, 7.5; magnetic field strength (P_e plot only), 10 teslas.

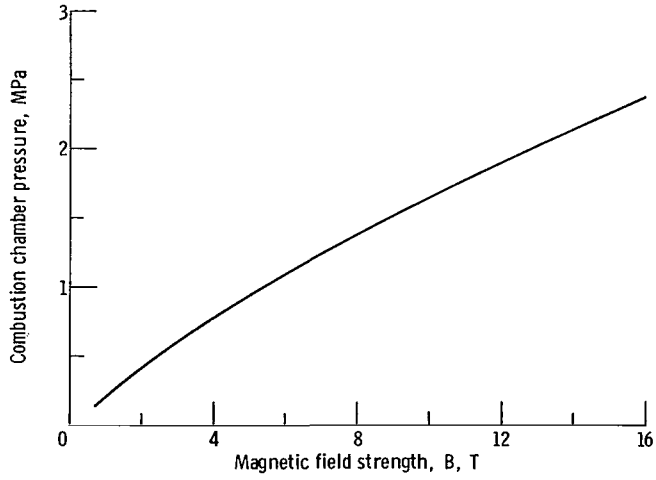

Figure 9. - Combustion pressure for maximum effective power density versus magnetic field. Oxygen to hydrogen weight ratio, 7.5; seed fraction, 3.5 mole percent.

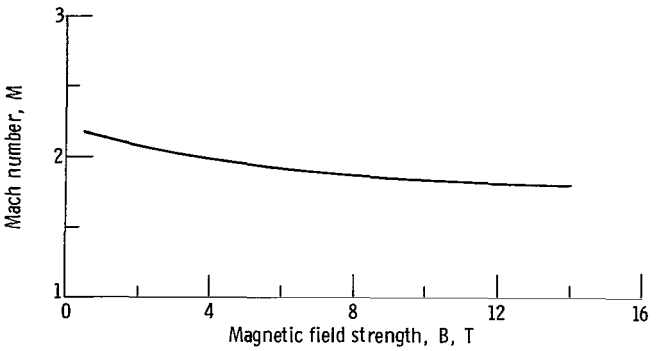

Figure 10. - Mach number for maximum effective power density versus magnetic field. Oxygen to hydrogen weight ratio, 7.5; seed fraction, 3.5 mole percent.

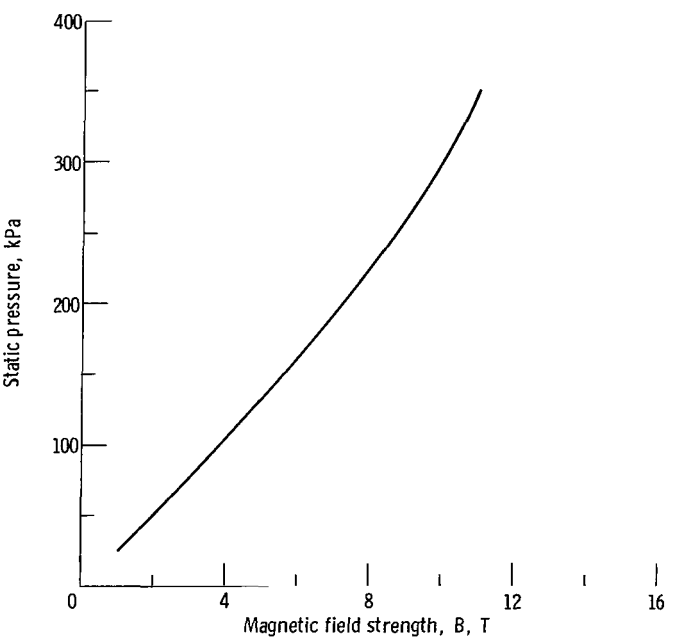

Figure 11. - Inlet static pressure for maximum effective power density versus magnetic field. Oxygen to hydrogen weight ratio, 7.5; seed fraction, 3.5 mole percent.

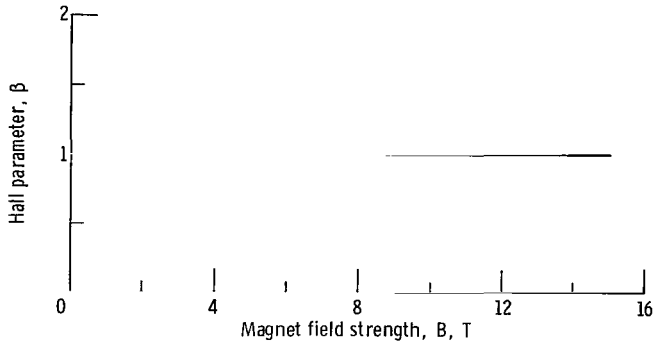

Figure 12. - Hall parameter for maximum effective power density versus magnetic field. Oxygen to hydrogen weight ratio, 7.5; seed fraction, 3.5 mole percent.

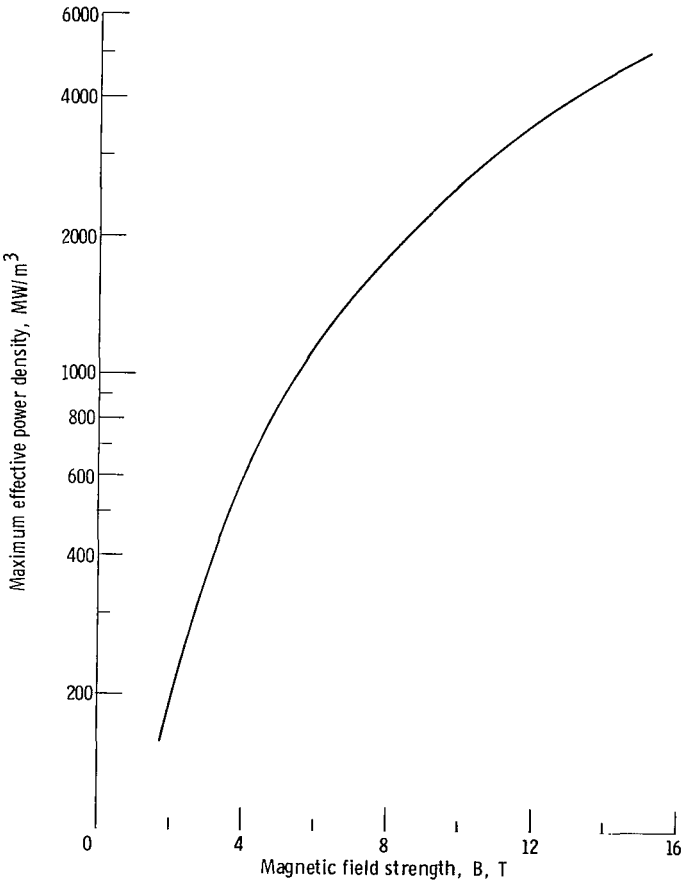

Figure 13. - Maximum effective power density versus magnetic field.

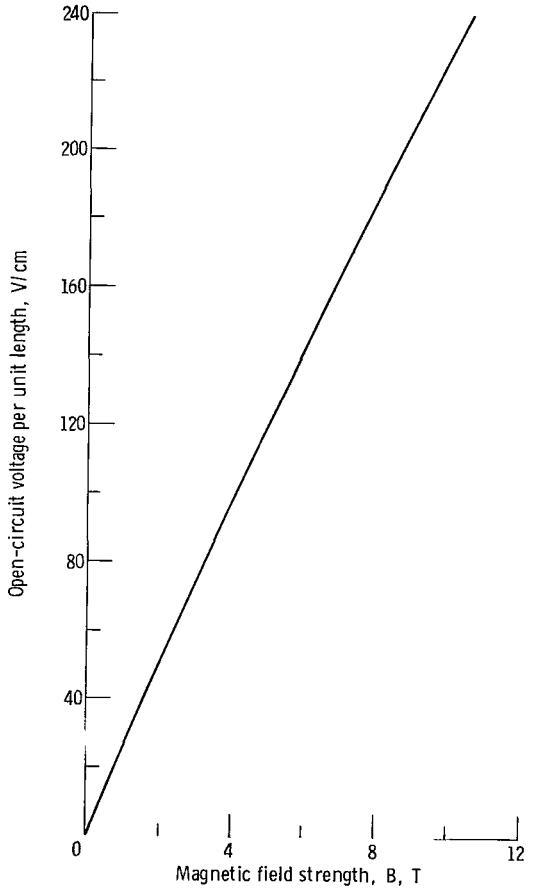

Figure 14. - Open-circuit voltage at maximum effective power density versus magnetic field. Oxygen to hydrogen weight ratio, 7.5; seed fraction, 3.5 mole percent.

"The aeronautical and space activities of the United States shall be conducted so as to contribute . . . to the expansion of human knowledge of phenomena in the atmosphere and space. The Administration shall provide for the widest practicable and appropriate dissemination of information concerning its activities and the results thereof."

—NATIONAL AERONAUTICS AND SPACE ACT OF 1958

NASA SCIENTIFIC AND TECHNICAL PUBLICATIONS

TECHNICAL REPORTS: Scientific and technical information considered important, complete, and a lasting contribution to existing knowledge.

TECHNICAL NOTES: Information less broad in scope but nevertheless of importance as a contribution to existing knowledge.

TECHNICAL MEMORANDUMS: Information receiving limited distribution because of preliminary data, security classification, or other reasons. Also includes conference proceedings with either limited or unlimited distribution.

CONTRACTOR REPORTS: Scientific and technical information generated under a NASA contract or grant and considered an important contribution to existing knowledge.

TECHNICAL TRANSLATIONS: Information published in a foreign language considered to merit NASA distribution in English.

SPECIAL PUBLICATIONS: Information derived from or of value to NASA activities. Publications include final reports of major projects, monographs, data compilations, handbooks, sourcebooks, and special bibliographies.

TECHNOLOGY UTILIZATION PUBLICATIONS: Information on technology used by NASA that may be of particular interest in commercial and other non-aerospace applications. Publications include Tech Briefs, Technology Utilization Reports and Technology Surveys.

Details on the availability of these publications may be obtained from:

SCIENTIFIC AND TECHNICAL INFORMATION OFFICE

NATIONAL AERONAUTICS AND SPACE ADMINISTRATION

Washington, D.C. 20546